PROCEEDINGS OF SCIENCE

ONLINE ICRC 2021
THE ASTROPARTICLE PHYSICS CONFERENCE
Berlin | Germany
37th International Cosmic Ray Conference
12–23 July 2021

Performance of the 433 m surface array of the Pierre Auger Observatory

Gaia Silli[a,b,*] **on behalf of the Pierre Auger**[c] **Collaboration**
(a complete list of authors can be found at the end of the proceedings)

[a] *Instituto de Tecnologías en Detección y Astropartículas (CNEA, CONICET, UNSAM), Av. General Paz 1555 (B1630KNA) San Martín, Buenos Aires, Argentina*
[b] *Institute for Astroparticle Physics (IAP), Karlsruhe Institute of Technology, P.O. Box 3640, 76021 Karlsruhe, Germany*
[c] *Observatorio Pierre Auger, Av. San Martín Norte 304, 5613 Malargüe, Argentina*
E-mail: spokespersons@auger.org

The Pierre Auger Observatory, located in western Argentina, is the world's largest cosmic-ray observatory. While it was originally built to study the cosmic-ray flux above $10^{18.5}$ eV, several enhancements have reduced this energy threshold. One such enhancement is a surface array composed of a triangular grid of 19 water-Cherenkov detectors separated by 433 m (SD-433) to explore the energies down to about 10^{16} eV. We are developing two research lines employing the SD-433. Firstly, we will measure the energy spectrum in a region where previous experiments have shown evidence of the second knee. Secondly, we will search for ultra-high energy photons to study PeV cosmic-ray sources residing in the Galactic center. In this work, we introduce the SD-433 and we show that it is fully efficient above 5×10^{16} eV for hadronic primaries with $\theta < 45°$. Using seven years of data, we present the parametrization of the lateral distribution function of measured signals. Finally, we show that an angular resolution of 1.8° (0.5°) can be attained at the lowest (highest) primary energies. Our study lays the goundmark for measurements in the energy range above 10^{16} eV by utilizing the SD-433 and thus expanding the scientific output of the Auger surface detector.

37th International Cosmic Ray Conference (ICRC 2021)
July 12th – 23rd, 2021
Online – Berlin, Germany

*Presenter

PoS(ICRC2021)224

1. Introduction

The detection of the cosmic-ray (CR) energy spectrum with surface detectors spans over six orders of magnitude in energy, from 10^{15} eV up to more than 10^{20} eV. It follows a power-law with a spectral index $\gamma \simeq 3$ exhibiting five features identified by small deviations in the spectral index: the knee, the second knee, the ankle, the "instep" [1], and a suppression at the highest energies. Particularly, the second knee has been observed at $\sim 10^{17}$ eV by several observatories as a steepening of the spectrum [2–6]. Its interpretation may be connected to the maximal energy of the accelerators in the Galaxy, considering that a gradual heavier composition has been observed at these energies [7], which is along the lines of the so-called Peters cycles [8]. The astrophysical interpretation of the acquired data is still delicate, mainly because the nature of the sources, the propagation effects, and the CR composition are strongly entwined. A signature of neutral particles such as photons and neutrinos around the second-knee may shed light on this problem, since they are not deflected by magnetic fields, thus providing valuable information about the acceleration processes in astrophysical objects.

A more accurate understanding of the origin of the second knee may be possible if one observatory is capable of measuring all spectral features and the CR mass composition with a common energy scale. In this sense, the Pierre Auger Observatory extended its Surface Detector (SD) with the deployment of a 433-m spaced triangular array (SD-433) of water-Cherenkov detectors (WCDs) to unveil the spectral region below 10^{17} eV. The installation of muon, radio, and surface scintillator stations within and around the SD-433, as part of the AugerPrime upgrade [9], allows us to perform a multi-detector measurement of the shower components. Additionally, the SD-433 is the detection platform to extend the search for ultra-high energy (UHE) photons from the southern hemisphere into the 10^{16} eV domain. A multi-messenger observation in this energy region is of utmost importance considering the discovery of PeVatrons in the Galactic center [10] and observations of UHE photons up to $\sim 10^{15}$ eV [11], while at the same time complementing the measurements of astrophysical neutrinos by the IceCube experiment [12].

In this work, we present the first studies about the detection performance of the SD-433 focussing on the energy range above 10^{16} eV. The status of the array, the simulation, and real data sets are described in Sec. 2. The probability of generating an array trigger from an air-shower with given primary parameters is discussed in Sec. 3. Sec. 4 is reserved for the evaluation of the distance at which the fluctuations of the measured signal in the WCDs are minimal. The modelling of the slope of the lateral distribution function (LDF) is detailed in Sec. 5. Sec. 6 encompasses the estimation of the resolution of the reconstructed air shower geometry. Finally, concluding comments embody Sec. 7.

2. Array description and data-set

The installation of the SD-433 array started in November 2011 with the deployment of a hexagon of WCDs around a central station, becoming fully operational in May 2013. The array achieved its final configuration consisting of 19 WCDs, thus reaching an aperture of $\sim 2\,\mathrm{km}^2$ sr up to $\theta = 45°$, on May 11, 2019. The 433-m array is surrounded by the 750-m array (SD-750) with

which it shares seven WCDs. At the same site, the location of the Underground Muon Detector (UMD) buried close to the WCDs is shown in Fig. 1.

The analysis of the array trigger efficiency was performed by simulating the response of the SD-433 to air showers. These were produced using CORSIKA 7.4950 with QGSJetII-04 and FLUKA as the high- and low-energy hadronic interaction model respectively. The simulation sample consisted of 2000 proton- and 2000 iron-initiated air showers. The primary particles followed a continuous energy distribution as E^{-1} between 4×10^{16} eV and 10^{17} eV and an isotropic distribution up to a zenith angle of $\theta = 55°$. The detector response was simulated employing the Offline framework of the Pierre Auger Collaboration [13]. Each shower core was randomly placed ten times within the unitary cell of the SD-433.

The remaining analyses were based on the real data acquired between May 2013 and May 2020. The response of the array to the impact of a shower front is defined hereafter as an event. Three conditions were required to select physical events among the background. Firstly, the event must have at least three triggered WCDs in a compact triangular configuration. Secondly, the six nearest WCDs around the one with the most intense signal must be operational (not necessarily triggered). Lastly, to ensure an unbiased estimation of the air-shower features, we selected events without any saturated WCDs. The final data-set was comprised by 115 thousand events.

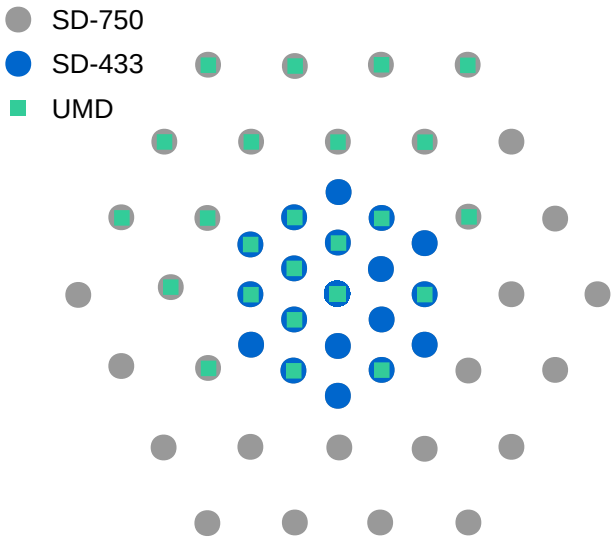

Figure 1: The schematic map of the SD-433. The complete array consists of two crowns (seven hexagons) of 19 WCDs spaced at 433 m.

3. Array efficiency

The array's efficiency ϵ is the probability of detecting an air shower by estimating the features of the primary particle. As such, it depends on the array spacing, the primary energy $E_{\rm MC}$, mass A, and the impinging zenith angle θ. Mathematically it is the ratio of the number of reconstructed events to the total tries. The efficiency can be parametrized as a function of the simulated primary energy $E_{\rm MC}$ as

$$\epsilon(E_{\rm MC}) = \frac{\mathrm{erf}\left(a \times \log_{10} \frac{E_{\rm MC}}{10^{16}\ \mathrm{eV}} + b\right) + 1}{2}, \tag{1}$$

and it is depicted in Fig. 2 for different zenith angle intervals between 0° and 55° for proton primaries and iron nuclei. Each efficiency curve is modeled by Eq. 1, represented in the figure as solid lines. It can be observed that the array becomes at least 97% efficient (i.e., defined as the full-efficiency regime) above $10^{16.7}$ eV for both primaries when considering $\theta < 45°$. Complementary, full-efficiency is attained above 10^{17} eV for larger zenith angles. Hence, the choice of a maximum

zenith angle of 45° is proposed. It is worth remarking that a lower energy threshold of $10^{16.5}$ eV can be reached when restricting the zenith angle up to $\theta = 35°$.

4. Optimal distance

The optimal distance r_{opt} is defined as the distance on the shower plane where the fluctuations of the LDF slope have the minimum influence on the average LDF. Stated otherwise, the signal provided by a model of average LDF at this distance is maximally reliable. This parameter depends on the array spacing [14] and can be estimated by varying the slope multiple times during the event reconstruction with an initial guess here chosen as 250 m. Technically, r_{opt} is then defined as the distance corresponding to the crossing point of these resulting fitted LDFs. Fig. 3 shows the distribution of the optimal distance for simulated and real data. The mean r_{opt} is estimated to be about 300 m independently of the zenith angle and the measured signal at 250 m. Recalling that the LDF, hence the shower footprint, is directly linked to the primary energy, it can be deduced that r_{opt} is also independent of the cosmic-ray energy. Similar distributions are obtained for simulated events with known primary composition as displayed in Fig. 3, right. Therefore, the optimal distance for the SD-433 is chosen as $r_{opt} = 300$ m.

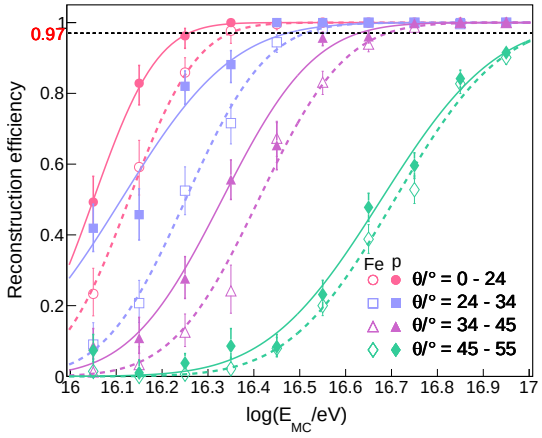

Figure 2: The reconstruction efficiency of the SD-433 in terms of the primary simulated energy for proton and iron primaries represented with solid and empty markers respectively, for different zenith angle intervals. The profiles are fitted with the model of Eq. 1.

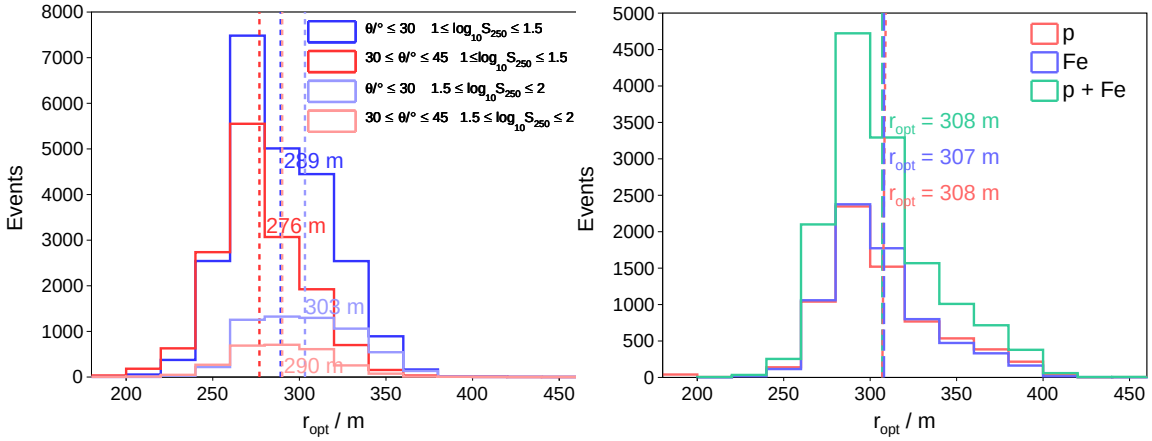

Figure 3: The r_{opt} distribution of reconstructed (left) and simulated (right) events. Stated and depicted with dashed vertical lines are the mean values of the histograms.

5. Lateral distribution function

The lateral distribution of signals measured with WCDs is customarily described by modified versions of the Nishimura-Kamata-Greisen (NKG) function:

$$S(r) = S(r_{\rm opt}) \cdot f_{\rm LDF}(r) = S(r_{\rm opt}) \cdot \left(\frac{r}{r_{\rm opt}}\right)^{\beta} \left(\frac{r + r_{\rm opt}}{r_{\rm scale} + r_{\rm opt}}\right)^{\beta}, \tag{2}$$

where by construction, the shape factor $f_{\rm LDF}$ is unity at the distance $r_{\rm opt}$, while the parameter β governs the expected signal drop with increasing distance. The scale parameter $r_{\rm scale}$ plays a role only at larger distances and has been kept fixed to 700 m. The normalization factor $S(r_{\rm opt})$ is the so-called shower size which is a measure of the primary energy. The model of average LDF is obtained by reconstructing the full set of real data leaving β as a free parameter to be fitted, which is possible if the event has at least five triggered stations. The event-by-event β can be described by a first degree polynomial in $\log_{10} S_{300}$. The functional form is

$$\beta(\log S_{300}, \theta) = a(\theta) + b(\theta) \times \log_{10} S_{300}\,, \tag{3}$$

where, in turn, the two coefficients follow a second degree polynomial in $\sec\theta$ given by

$$\begin{pmatrix} a \\ b \end{pmatrix} = \begin{pmatrix} -3.72 & 1.30 & 0.055 \\ 0.98 & -1.30 & 0.385 \end{pmatrix} \times \begin{pmatrix} 1 \\ \sec\theta \\ \sec^2\theta \end{pmatrix}. \tag{4}$$

After employing the selection and quality cuts stated in Sec. 2, the six fitted parameters are summarized in Eq. 4.

In Fig. 4, left, a comparison of the event-by-event fitted slope β_i (markers) and the model prediction $\tilde{\beta}_i$ (solid lines) is shown. In order to evaluate the goodness of the parametrization, it is instructive to look at the residuals in Fig. 4, right. It can be observed that the model gives an accurate description of the data with an average relative difference of the order of 2% for the considered zenith angle range.

Since the average LDF slope can be fixed by the mentioned parametrization, a similar procedure can be conducted for its fluctuations. The β distribution follows a Gaussian probability density function when limited to a certain energy interval or, analogously, to a shower size interval. Thus the uncertainty can be represented as the standard deviation of the mean of the Gaussian distribution. In this sense, Fig. 5 shows the uncertainty of the parametrized β as a function of the shower size. The slope uncertainty model is defined by

$$\sigma_\beta = \exp\left[p_0 + p_1 \cdot \log_{10}(S_{300}/\mathrm{VEM})\right], \tag{5}$$

with fitted parameters $p_0 = (0.01 \pm 0.02)$ and $p_1 = (1.2 \pm 0.02)$.

6. Geometry resolution

The uncertainty of the reconstructed core position can be characterized by the variance of each coordinate of the impact point, σ_x^2 and σ_y^2, plus the covariance between them $\mathrm{cov}(x, y)$. To

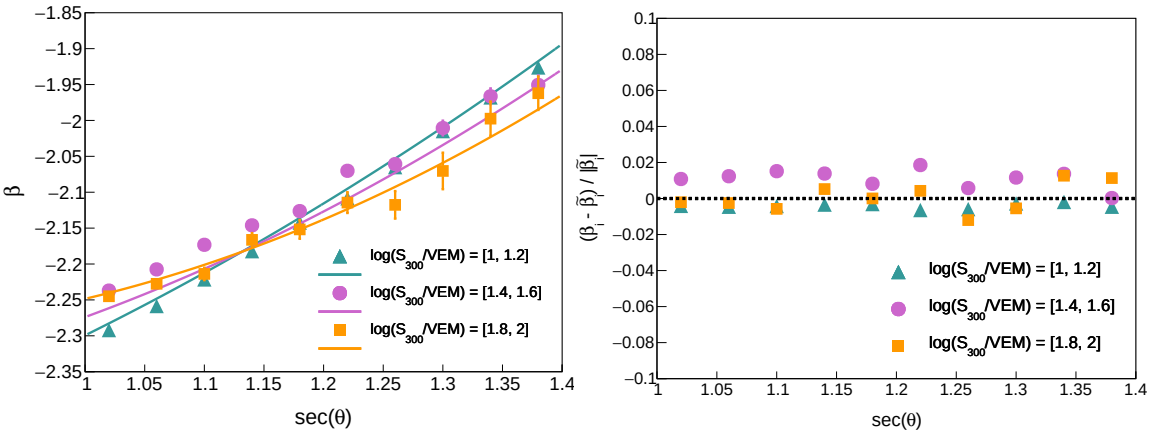

Figure 4: Left: The event-by-event fitted β and the superimposed model predictions by means of Eq. 2 in terms of the sec θ for the quoted shower size intervals. Right: the relative differences between fitted data and the model prediction of β.

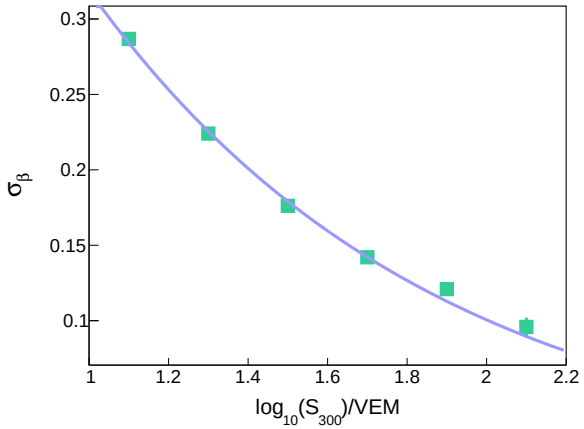

Figure 5: The uncertainty of the parametrized β in terms of the shower size S_{300} for events with $\theta < 45°$.

concentrate the three quantities into a single parameter, we can use the distance r between the hottest WCD and the shower axis. Its variance, σ_r^2, is calculated as

$$\sigma_r^2 = \frac{1}{r^2} \times ((x - x_{\rm hot})^2 \cdot \sigma_x^2 + (y - y_{\rm hot})^2 \cdot \sigma_y^2 + 2 \cdot (x - x_{\rm hot}) \cdot (y - y_{\rm hot}) \cdot {\rm cov}(x, y)) \,. \quad (6)$$

The core position resolution Σ_r is regarded as the 68%-quantile of the resulting σ_r distribution. In the case of the angular resolution, a closed formula for the event-by-event angular resolution Σ_η can be obtained from the variances of the reconstructed zenith (θ) and azimuth (ϕ) angles [15] as

$$\Sigma_\eta = \sqrt{-\ln(1 - 0.68) \times (\sigma_\theta^2 + \sin^2\theta \cdot \sigma_\phi^2)} \,. \quad (7)$$

The median of the Σ_η for each $S_{300} - \theta$ bin is reported as the angular resolution.

The evolution of the core and angular resolution in terms of the shower size S_{300} is displayed in Fig. 6. In both cases, there is a zenith dependence coming from the shower size, i.e., an inclined

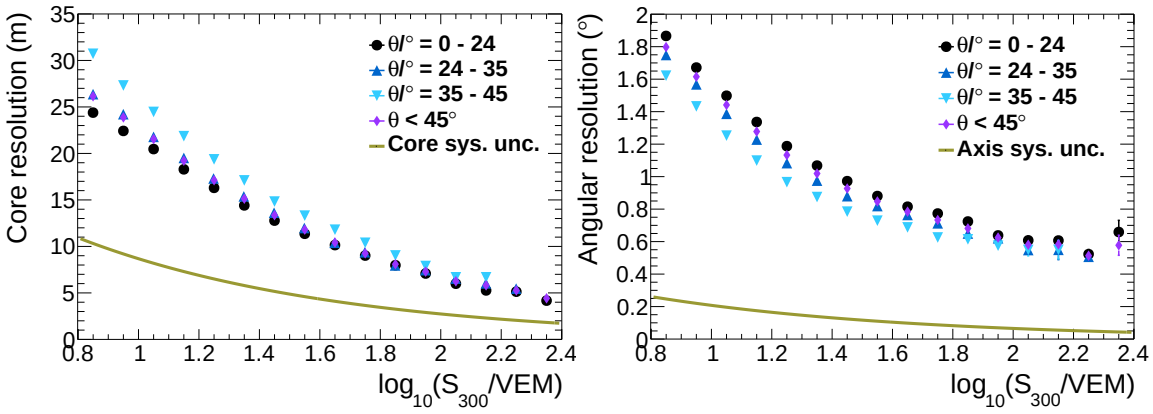

Figure 6: The core position resolution (left) and angular resolution (right) in terms of the shower size after applying the selection cuts described in Sec. 2. The systematic uncertainty on each observable due to the uncertainty of the LDF slope (see Fig. 5) is represented by the solid dark-yellow lines.

high-energy event may be measured with a shower size similar to that of a vertical low-energy event. On the one hand, the core resolution decreases at more inclined directions due to the intrinsic smearing in a flatter shower front for older showers. On the other hand, the angular resolution follows the opposite behavior which may be explained by the mentioned energy mixing. Overall a better resolution in both parameters is attained as the signal footprint size increases, i.e., with a higher multiplicity probing of the shower front. The angular resolution is enhanced up to the degree level at $S_{300} \sim 22$ VEM roughly corresponding to an equivalent simulated energy of $10^{16.7}$ eV. The systematic uncertainty on the shower axis, propagated from the uncertainty on the LDF slope (see Fig. 5), is less than 0.3°. The angular resolution deteriorates with a decreasing shower size down to 1.8° at $S_{300} \sim 7$ VEM, which corresponds to simulated energies at the verge of the full-efficiency regime.

7. Discussion

The SD-433 array provides the opportunity to extend the sensitivity of the Auger surface detector down to 10^{16} eV. By means of Monte-Carlo simulations, we reported a full-efficiency threshold of $10^{16.5}$ eV for proton and $10^{16.6}$ eV for iron primaries up to $\theta = 45°$. Thus, the SD-433 offers the possibility to fully observe the second-knee feature in the CR spectrum, previously reported around 10^{17} eV, with full reconstruction efficiency.

We employed the seven-year data-set to develop the steps of the event reconstruction process. Firstly, we found that the distance of minimum LDF fluctuations is 300 m at all energies and zenith angles of interest. The value of the average LDF at this distance is the observable that reflects the primary energy with the best resolution. To provide a more stable event reconstruction, we presented a six-parameter parametrization of the LDF slope which correctly described the event-by-event fitted slope, when the event geometry is favorable to perform this fit, within 2% at all energies of interest. Lastly, the characterization of the geometric accuracy of the SD-433 has been presented. An angular resolution better than $\sim$ 1.8° has been found, which may suffice to allow

large-scale directional studies in the 10^{16} eV domain, e.g., search for UHE photons coming from Galactic PeVatron sources allocated in the Galactic center and from off-plane directions compatible with the Fermi bubbles and the dark-matter halo.

The fine-tuning of the SD-433 event reconstruction is still ongoing. The transformation from the zenith-dependent shower size to the estimated primary energy requires a study of the atmospheric attenuation and the weather-induced modulations on the measured signals prior to the calibration of the shower size with an independent measurement of the primary energy.

This analysis will set the foundations for extending the SD-oriented research lines in Auger to energies down to 10^{16} eV.

References

[1] A. Aab et al. [Pierre Auger Coll.], *Phys. Rev. D 102, 062005* 2020,
[2] The Telescope Array Coll. Astrophys. J., 865(1), 2018.
[3] V. Novotný [for the Pierre Auger Coll.], these proceedings.
[4] K. Rawlins for the IceCube Coll. J. Phys. Conf. Ser. 718 052033, 2018.
[5] The Kascade-Grande Coll. Astropart. Phys. 36 183, 2012.
[6] A. Aab et al. [Pierre Auger Coll.], "The energy spectrum of cosmic rays beyond the turn-down around 10^{17} eV as measured with the surface detector of the Pierre Auger Observatory". To be submitted to Eur. Phys. J. C
[7] K-H. Kampert and M. Unger. Astropart. Phys., 35(10) 660–678, 2012.
[8] B. Peters. *Nuovo Cim. 22, 800–819* 1961,
[9] A. Castellina [for the Pierre Auger Coll.]. EPJ Web Conf. 210 06002, 2019.
[10] The Tibet AS-γ Coll. Phys. Rev. Lett. 126, 141101, 2021.
[11] The LHAASO Coll. Nature, 2021.
[12] The IceCube Coll. Phys. Rev. Lett. 111, 021103, 2013.
[13] L. Nellen [for the Pierre Auger Coll.], these proceedings.
[14] D. Newton, J. Knapp and A. Watson. Astropart. Phys. 26 414-419, 2007.
[15] C. Bonifazi [for the Pierre Auger Coll.], Nucl. Phys. B Proc. Suppl. 190:20–25, 2009.

PoS(ICRC2021)224

The Pierre Auger Collaboration

P. Abreu[72], M. Aglietta[54,52], J.M. Albury[13], I. Allekotte[1], A. Almela[8,12], J. Alvarez-Muñiz[79], R. Alves Batista[80], G.A. Anastasi[63,52], L. Anchordoqui[87], B. Andrada[8], S. Andringa[72], C. Aramo[50], P.R. Araújo Ferreira[42], J. C. Arteaga Velázquez[67], H. Asorey[8], P. Assis[72], G. Avila[11], A.M. Badescu[75], A. Bakalova[32], A. Balaceanu[73], F. Barbato[45,46], R.J. Barreira Luz[72], K.H. Becker[38], J.A. Bellido[13,69], C. Berat[36], M.E. Bertaina[63,52], X. Bertou[1], P.L. Biermann[b], V. Binet[6], K. Bismark[39,8], T. Bister[42], J. Biteau[37], J. Blazek[32], C. Bleve[36], M. Boháčová[32], D. Boncioli[57,46], C. Bonifazi[9,26], L. Bonneau Arbeletche[21], N. Borodai[70], A.M. Botti[8], J. Brack[d], T. Bretz[42], P.G. Brichetto Orchera[8], F.L. Briechle[42], P. Buchholz[44], A. Bueno[78], S. Buitink[15], M. Buscemi[47], M. Büsken[39,8], K.S. Caballero-Mora[66], L. Caccianiga[59,49], F. Canfora[80,81], I. Caracas[38], J.M. Carceller[78], R. Caruso[58,47], A. Castellina[54,52], F. Catalani[19], G. Cataldi[48], L. Cazon[72], M. Cerda[10], J.A. Chinellato[22], J. Chudoba[32], L. Chytka[33], R.W. Clay[13], A.C. Cobos Cerutti[7], R. Colalillo[60,50], A. Coleman[93], M.R. Coluccia[48], R. Conceição[72], A. Condorelli[45,46], G. Consolati[49,55], F. Contreras[11], F. Convenga[56,48], D. Correia dos Santos[28], C.E. Covault[85], S. Dasso[5,3], K. Daumiller[41], B.R. Dawson[13], J.A. Day[13], R.M. de Almeida[28], J. de Jesús[8,41], S.J. de Jong[80,81], G. De Mauro[80,81], J.R.T. de Mello Neto[26,27], I. De Mitri[45,46], J. de Oliveira[18], D. de Oliveira Franco[22], F. de Palma[56,48], V. de Souza[20], E. De Vito[56,48], M. del Río[11], O. Deligny[34], L. Deval[41,8], A. di Matteo[52], C. Dobrigkeit[22], J.C. D'Olivo[68], L.M. Domingues Mendes[72], R.C. dos Anjos[25], D. dos Santos[28], M.T. Dova[4], J. Ebr[32], R. Engel[39,41], I. Epicoco[56,48], M. Erdmann[42], C.O. Escobar[a], A. Etchegoyen[8,12], H. Falcke[80,82,81], J. Farmer[92], G. Farrar[90], A.C. Fauth[22], N. Fazzini[a], F. Feldbusch[40], F. Fenu[54,52], B. Fick[89], J.M. Figueira[8], A. Filipčič[77,76], T. Fitoussi[41], T. Fodran[80], M.M. Freire[6], T. Fujii[92,e], A. Fuster[8,12], C. Galea[80], C. Galelli[59,49], B. García[7], A.L. Garcia Vegas[42], H. Gemmeke[40], F. Gesualdi[8,41], A. Gherghel-Lascu[73], P.L. Ghia[34], U. Giaccari[80], M. Giammarchi[49], J. Glombitza[42], F. Gobbi[10], F. Gollan[8], G. Golup[1], M. Gómez Berisso[1], P.F. Gómez Vitale[11], J.P. Gongora[11], J.M. González[1], N. González[14], I. Goos[1,41], D. Góra[70], A. Gorgi[54,52], M. Gottowik[38], T.D. Grubb[13], F. Guarino[60,50], G.P. Guedes[23], E. Guido[52,63], S. Hahn[41,8], P. Hamal[32], M.R. Hampel[8], P. Hansen[4], D. Harari[1], V.M. Harvey[13], A. Haungs[41], T. Hebbeker[42], D. Heck[41], G.C. Hill[13], C. Hojvat[a], J.R. Hörandel[80,81], P. Horvath[33], M. Hrabovský[33], T. Huege[41,15], A. Insolia[58,47], P.G. Isar[74], P. Janecek[32], J.A. Johnsen[86], J. Jurysek[32], A. Kääpä[38], K.H. Kampert[38], N. Karastathis[41], B. Keilhauer[41], J. Kemp[42], A. Khakurdikar[80], V.V. Kizakke Covilakam[8,41], H.O. Klages[41], M. Kleifges[40], J. Kleinfeller[10], M. Köpke[39], N. Kunka[40], B.L. Lago[17], R.G. Lang[20], N. Langner[42], M.A. Leigui de Oliveira[24], V. Lenok[41], A. Letessier-Selvon[35], I. Lhenry-Yvon[34], D. Lo Presti[58,47], L. Lopes[72], R. López[64], L. Lu[94], Q. Luce[39], J.P. Lundquist[76], A. Machado Payeras[22], G. Mancarella[56,48], D. Mandat[32], B.C. Manning[13], J. Manshanden[43], P. Mantsch[a], S. Marafico[34], A.G. Mariazzi[4], I.C. Mariş[14], G. Marsella[61,47], D. Martello[56,48], S. Martinelli[41,8], O. Martínez Bravo[64], M. Mastrodicasa[57,46], H.J. Mathes[41], J. Matthews[88], G. Matthiae[62,51], E. Mayotte[38], P.O. Mazur[a], G. Medina-Tanco[68], D. Melo[8], A. Menshikov[40], K.-D. Merenda[86], S. Michal[33], M.I. Micheletti[6], L. Miramonti[59,49], S. Mollerach[1], F. Montanet[36], C. Morello[54,52], M. Mostafá[91], A.L. Müller[8], M.A. Muller[22], K. Mulrey[15], R. Mussa[52], M. Muzio[90], W.M. Namasaka[38], A. Nasr-Esfahani[38], L. Nellen[68], M. Niculescu-Oglinzanu[73], M. Niechciol[44], D. Nitz[89], D. Nosek[31], V. Novotny[31], L. Nožka[33], A Nucita[56,48], L.A. Núñez[30], M. Palatka[32], J. Pallotta[2], P. Papenbreer[38], G. Parente[79], A. Parra[64], J. Pawlowsky[38], M. Pech[32], F. Pedreira[79], J. Pękala[70], R. Pelayo[65], J. Peña-Rodriguez[30], E.E. Pereira Martins[39,8], J. Perez Armand[21], C. Pérez Bertolli[8,41], M. Perlin[8,41], L. Perrone[56,48], S. Petrera[45,46], T. Pierog[41], M. Pimenta[72], V. Pirronello[58,47], M. Platino[8], B. Pont[80], M. Pothast[81,80], P. Privitera[92], M. Prouza[32], A. Puyleart[89], S. Querchfeld[38], J. Rautenberg[38], D. Ravignani[8], M. Reininghaus[41,8], J. Ridky[32], F. Riehn[72], M. Risse[44], V. Rizi[57,46], W. Rodrigues de Carvalho[21], J. Rodriguez Rojo[11], M.J. Roncoroni[8], S. Rossoni[43], M. Roth[41], E. Roulet[1], A.C. Rovero[5], P. Ruehl[44], A. Saftoiu[73], F. Salamida[57,46], H. Salazar[64], G. Salina[51], J.D. Sanabria Gomez[30], F. Sánchez[8], E.M. Santos[21], E. Santos[32], F. Sarazin[86], R. Sarmento[72], C. Sarmiento-Cano[8], R. Sato[11],

P. Savina[56,48,34,94], C.M. Schäfer[41], V. Scherini[56,48], H. Schieler[41], M. Schimassek[39,8], M. Schimp[38], F. Schlüter[41,8], D. Schmidt[39], O. Scholten[84,15], P. Schovánek[32], F.G. Schröder[93,41], S. Schröder[38], J. Schulte[42], S.J. Sciutto[4], M. Scornavacche[8,41], A. Segreto[53,47], S. Sehgal[38], R.C. Shellard[16], G. Sigl[43], G. Silli[8,41], O. Sima[73,f], R. Šmída[92], P. Sommers[91], J.F. Soriano[87], J. Souchard[36], R. Squartini[10], M. Stadelmaier[41,8], D. Stanca[73], S. Stanič[76], J. Stasielak[70], P. Stassi[36], A. Streich[39,8], M. Suárez-Durán[14], T. Sudholz[13], T. Suomijärvi[37], A.D. Supanitsky[8], Z. Szadkowski[71], A. Tapia[29], C. Taricco[63,52], C. Timmermans[81,80], O. Tkachenko[41], P. Tobiska[32], C.J. Todero Peixoto[19], B. Tomé[72], Z. Torrès[36], A. Travaini[10], P. Travnicek[32], C. Trimarelli[57,46], M. Tueros[4], R. Ulrich[41], M. Unger[41], L. Vaclavek[33], M. Vacula[33], J.F. Valdés Galicia[68], L. Valore[60,50], E. Varela[64], A. Vásquez-Ramírez[30], D. Veberič[41], C. Ventura[27], I.D. Vergara Quispe[4], V. Verzi[51], J. Vicha[32], J. Vink[83], S. Vorobiov[76], H. Wahlberg[4], C. Watanabe[26], A.A. Watson[c], M. Weber[40], A. Weindl[41], L. Wiencke[86], H. Wilczyński[70], M. Wirtz[42], D. Wittkowski[38], B. Wundheiler[8], A. Yushkov[32], O. Zapparrata[14], E. Zas[79], D. Zavrtanik[76,77], M. Zavrtanik[77,76], L. Zehrer[76]

———— • ————

[1] Centro Atómico Bariloche and Instituto Balseiro (CNEA-UNCuyo-CONICET), San Carlos de Bariloche, Argentina
[2] Centro de Investigaciones en Láseres y Aplicaciones, CITEDEF and CONICET, Villa Martelli, Argentina
[3] Departamento de Física and Departamento de Ciencias de la Atmósfera y los Océanos, FCEyN, Universidad de Buenos Aires and CONICET, Buenos Aires, Argentina
[4] IFLP, Universidad Nacional de La Plata and CONICET, La Plata, Argentina
[5] Instituto de Astronomía y Física del Espacio (IAFE, CONICET-UBA), Buenos Aires, Argentina
[6] Instituto de Física de Rosario (IFIR) – CONICET/U.N.R. and Facultad de Ciencias Bioquímicas y Farmacéuticas U.N.R., Rosario, Argentina
[7] Instituto de Tecnologías en Detección y Astropartículas (CNEA, CONICET, UNSAM), and Universidad Tecnológica Nacional – Facultad Regional Mendoza (CONICET/CNEA), Mendoza, Argentina
[8] Instituto de Tecnologías en Detección y Astropartículas (CNEA, CONICET, UNSAM), Buenos Aires, Argentina
[9] International Center of Advanced Studies and Instituto de Ciencias Físicas, ECyT-UNSAM and CONICET, Campus Miguelete – San Martín, Buenos Aires, Argentina
[10] Observatorio Pierre Auger, Malargüe, Argentina
[11] Observatorio Pierre Auger and Comisión Nacional de Energía Atómica, Malargüe, Argentina
[12] Universidad Tecnológica Nacional – Facultad Regional Buenos Aires, Buenos Aires, Argentina
[13] University of Adelaide, Adelaide, S.A., Australia
[14] Université Libre de Bruxelles (ULB), Brussels, Belgium
[15] Vrije Universiteit Brussels, Brussels, Belgium
[16] Centro Brasileiro de Pesquisas Fisicas, Rio de Janeiro, RJ, Brazil
[17] Centro Federal de Educação Tecnológica Celso Suckow da Fonseca, Nova Friburgo, Brazil
[18] Instituto Federal de Educação, Ciência e Tecnologia do Rio de Janeiro (IFRJ), Brazil
[19] Universidade de São Paulo, Escola de Engenharia de Lorena, Lorena, SP, Brazil
[20] Universidade de São Paulo, Instituto de Física de São Carlos, São Carlos, SP, Brazil
[21] Universidade de São Paulo, Instituto de Física, São Paulo, SP, Brazil
[22] Universidade Estadual de Campinas, IFGW, Campinas, SP, Brazil
[23] Universidade Estadual de Feira de Santana, Feira de Santana, Brazil
[24] Universidade Federal do ABC, Santo André, SP, Brazil
[25] Universidade Federal do Paraná, Setor Palotina, Palotina, Brazil
[26] Universidade Federal do Rio de Janeiro, Instituto de Física, Rio de Janeiro, RJ, Brazil
[27] Universidade Federal do Rio de Janeiro (UFRJ), Observatório do Valongo, Rio de Janeiro, RJ, Brazil
[28] Universidade Federal Fluminense, EEIMVR, Volta Redonda, RJ, Brazil
[29] Universidad de Medellín, Medellín, Colombia
[30] Universidad Industrial de Santander, Bucaramanga, Colombia
[31] Charles University, Faculty of Mathematics and Physics, Institute of Particle and Nuclear Physics, Prague, Czech Republic
[32] Institute of Physics of the Czech Academy of Sciences, Prague, Czech Republic

[33] Palacky University, RCPTM, Olomouc, Czech Republic
[34] CNRS/IN2P3, IJCLab, Université Paris-Saclay, Orsay, France
[35] Laboratoire de Physique Nucléaire et de Hautes Energies (LPNHE), Sorbonne Université, Université de Paris, CNRS-IN2P3, Paris, France
[36] Univ. Grenoble Alpes, CNRS, Grenoble Institute of Engineering Univ. Grenoble Alpes, LPSC-IN2P3, 38000 Grenoble, France
[37] Université Paris-Saclay, CNRS/IN2P3, IJCLab, Orsay, France
[38] Bergische Universität Wuppertal, Department of Physics, Wuppertal, Germany
[39] Karlsruhe Institute of Technology (KIT), Institute for Experimental Particle Physics, Karlsruhe, Germany
[40] Karlsruhe Institute of Technology (KIT), Institut für Prozessdatenverarbeitung und Elektronik, Karlsruhe, Germany
[41] Karlsruhe Institute of Technology (KIT), Institute for Astroparticle Physics, Karlsruhe, Germany
[42] RWTH Aachen University, III. Physikalisches Institut A, Aachen, Germany
[43] Universität Hamburg, II. Institut für Theoretische Physik, Hamburg, Germany
[44] Universität Siegen, Department Physik – Experimentelle Teilchenphysik, Siegen, Germany
[45] Gran Sasso Science Institute, L'Aquila, Italy
[46] INFN Laboratori Nazionali del Gran Sasso, Assergi (L'Aquila), Italy
[47] INFN, Sezione di Catania, Catania, Italy
[48] INFN, Sezione di Lecce, Lecce, Italy
[49] INFN, Sezione di Milano, Milano, Italy
[50] INFN, Sezione di Napoli, Napoli, Italy
[51] INFN, Sezione di Roma "Tor Vergata", Roma, Italy
[52] INFN, Sezione di Torino, Torino, Italy
[53] Istituto di Astrofisica Spaziale e Fisica Cosmica di Palermo (INAF), Palermo, Italy
[54] Osservatorio Astrofisico di Torino (INAF), Torino, Italy
[55] Politecnico di Milano, Dipartimento di Scienze e Tecnologie Aerospaziali , Milano, Italy
[56] Università del Salento, Dipartimento di Matematica e Fisica "E. De Giorgi", Lecce, Italy
[57] Università dell'Aquila, Dipartimento di Scienze Fisiche e Chimiche, L'Aquila, Italy
[58] Università di Catania, Dipartimento di Fisica e Astronomia, Catania, Italy
[59] Università di Milano, Dipartimento di Fisica, Milano, Italy
[60] Università di Napoli "Federico II", Dipartimento di Fisica "Ettore Pancini", Napoli, Italy
[61] Università di Palermo, Dipartimento di Fisica e Chimica "E. Segrè", Palermo, Italy
[62] Università di Roma "Tor Vergata", Dipartimento di Fisica, Roma, Italy
[63] Università Torino, Dipartimento di Fisica, Torino, Italy
[64] Benemérita Universidad Autónoma de Puebla, Puebla, México
[65] Unidad Profesional Interdisciplinaria en Ingeniería y Tecnologías Avanzadas del Instituto Politécnico Nacional (UPIITA-IPN), México, D.F., México
[66] Universidad Autónoma de Chiapas, Tuxtla Gutiérrez, Chiapas, México
[67] Universidad Michoacana de San Nicolás de Hidalgo, Morelia, Michoacán, México
[68] Universidad Nacional Autónoma de México, México, D.F., México
[69] Universidad Nacional de San Agustin de Arequipa, Facultad de Ciencias Naturales y Formales, Arequipa, Peru
[70] Institute of Nuclear Physics PAN, Krakow, Poland
[71] University of Łódź, Faculty of High-Energy Astrophysics,Łódź, Poland
[72] Laboratório de Instrumentação e Física Experimental de Partículas – LIP and Instituto Superior Técnico – IST, Universidade de Lisboa – UL, Lisboa, Portugal
[73] "Horia Hulubei" National Institute for Physics and Nuclear Engineering, Bucharest-Magurele, Romania
[74] Institute of Space Science, Bucharest-Magurele, Romania
[75] University Politehnica of Bucharest, Bucharest, Romania
[76] Center for Astrophysics and Cosmology (CAC), University of Nova Gorica, Nova Gorica, Slovenia
[77] Experimental Particle Physics Department, J. Stefan Institute, Ljubljana, Slovenia
[78] Universidad de Granada and C.A.F.P.E., Granada, Spain
[79] Instituto Galego de Física de Altas Enerxías (IGFAE), Universidade de Santiago de Compostela, Santiago de Compostela, Spain

PoS(ICRC2021)224

[80] IMAPP, Radboud University Nijmegen, Nijmegen, The Netherlands
[81] Nationaal Instituut voor Kernfysica en Hoge Energie Fysica (NIKHEF), Science Park, Amsterdam, The Netherlands
[82] Stichting Astronomisch Onderzoek in Nederland (ASTRON), Dwingeloo, The Netherlands
[83] Universiteit van Amsterdam, Faculty of Science, Amsterdam, The Netherlands
[84] University of Groningen, Kapteyn Astronomical Institute, Groningen, The Netherlands
[85] Case Western Reserve University, Cleveland, OH, USA
[86] Colorado School of Mines, Golden, CO, USA
[87] Department of Physics and Astronomy, Lehman College, City University of New York, Bronx, NY, USA
[88] Louisiana State University, Baton Rouge, LA, USA
[89] Michigan Technological University, Houghton, MI, USA
[90] New York University, New York, NY, USA
[91] Pennsylvania State University, University Park, PA, USA
[92] University of Chicago, Enrico Fermi Institute, Chicago, IL, USA
[93] University of Delaware, Department of Physics and Astronomy, Bartol Research Institute, Newark, DE, USA
[94] University of Wisconsin-Madison, Department of Physics and WIPAC, Madison, WI, USA

—

[a] Fermi National Accelerator Laboratory, Fermilab, Batavia, IL, USA
[b] Max-Planck-Institut für Radioastronomie, Bonn, Germany
[c] School of Physics and Astronomy, University of Leeds, Leeds, United Kingdom
[d] Colorado State University, Fort Collins, CO, USA
[e] now at Hakubi Center for Advanced Research and Graduate School of Science, Kyoto University, Kyoto, Japan
[f] also at University of Bucharest, Physics Department, Bucharest, Romania

PoS(ICRC2021)224